FRONT MATTER

Nuclear assembly in giant unilamellar vesicles encapsulating *Xenopus* egg extract

Authors

Sho Takamori[1], Hisatoshi Mimura[1], Toshihisa Osaki[1], Tomo Kondo[2]†, Miyuki Shintomi[3], Keishi Shintomi[4], Miho Ohsugi[2]†, Shoji Takeuchi[1,5,6]*

Affiliations

[1]Artificial Cell Membrane Systems Group, Kanagawa Institute of Industrial Science and Technology, 3-2-1 Sakado, Takatsu-ku, Kawasaki, Kanagawa 213-0012, Japan.

[2]Department of Life Science, Graduate School of Arts and Sciences, The University of Tokyo, Meguro-ku, Tokyo 153-8902, Japan.

[3]Life Science Network, The University of Tokyo, Meguro-ku, Tokyo 153-8902, Japan.

[4]Chromosome Dynamics Laboratory, RIKEN, Wako, Saitama 351-0198, Japan.

[5]Institute of Industrial Science, The University of Tokyo, 4-6-1 Komaba, Meguro-ku, Tokyo 153-8505, Japan.

[6]Department of Mechano-Informatics, Graduate School of Information Science and Technology, The University of Tokyo, 7-3-1 Hongo, Bunkyo-ku, Tokyo 113-8656, Japan.

†Present address: Department of Biological Sciences, Graduate School of Science, The University of Tokyo, 7-3-1 Hongo, Bunkyo-ku, Tokyo 113-0033, Japan.

*Corresponding author. Email: takeuchi@hybrid.t.u-tokyo.ac.jp

Abstract

The reconstitution of a cell nucleus in a lipid bilayer-enclosed synthetic cell makes great strides in bottom-up synthetic biology. In this study, we propose a method for assembling a nucleus in giant unilamellar vesicles (GUVs). To induce reconstitution of the nucleus, we utilize interphase egg extract of African clawed frogs *Xenopus laevis*, known as a biochemically controllable cell-free system capable of transforming an added sperm chromatin into a nucleus *in vitro*. We enhanced GUV formation efficiency by the inverted emulsion method through incorporating prolonged waiting time and adding chloroform into lipid-dispersed oil, facilitating subsequent nuclear assembly reactions in the GUVs. Characterization of nucleus-like structures formed in the GUVs revealed the presence of dense DNA and accumulated GFP-NLS in the structure, indicative of functional nuclear import. Immunostaining further validated the presence of nuclear pore complexes on the surfaces of these nucleus-like structures. Our approach offers a versatile platform for constructing artificial cellular systems that closely mimic eukaryotic cells.

Teaser

A cell nucleus is reconstituted in lipid bilayer-enclosed confinements using egg extract from African clawed frogs.

MAIN TEXT

Introduction

Cell nucleus serves as a crucial subcellular compartment in eukaryotic cells, responsible for overseeing the maintenance of genetic materials and orchestrating their functions. Recent advancements in bottom-up synthetic biology have focused on constructing or integrating cell-like functional subcellular compartments in synthetic cells (*1-5*). These efforts aim to replicate the functions of natural subcellular compartments such as photosynthesis in chloroplasts (*6-8*), mitochondrial respiration (*9-11*), and spatial organization of gene expression reactions in the nucleus (*12-13*). Among various eukaryotic subcellular compartments, the nucleus stands out as a central element in the regulation of eukaryotic cellular processes. Constructing the nucleus in synthetic cells encapsulated with a lipid bilayer represents a significant stride towards developing artificial eukaryotic cellular structures (*14*). Reconstitution of natural cell nucleus has previously been achieved in bulk solution (*15-17*), microfluidic devices (*18,19*), and water-in-oil emulsions (*20-22*), by utilizing egg extracts of the African clawed frog *Xenopus laevis*. The "interphase" egg extract of *Xenopus laevis* is known as a biochemically manipulable cell-free system, capable of transforming sperm chromatin into a nucleus *in vitro* (*15-17*). However, the challenge of assembling the nucleus in a lipid bilayer-enclosed confinement remains unmet. While encapsulation of an unspecified type of the egg extract into lipid bilayer-enclosed confinement has previously been reported (*23*), the typical yield in encapsulation of the interphase egg extract is low. This low yield can be attributed to the reported destabilization of the lipid bilayer in the presence of *Xenopus* egg extract (*24*), highlighting the challenge of achieving stability in the lipid membrane surrounding the egg extract. Thus, stabilizing the lipid bilayer could significantly improve the efficiency of encapsulation and enable the reconstitution of a nucleus in cell-like confinement enclosed with a lipid membrane.

In this study, we reconstitute a cell nucleus in giant unilamellar vesicles (GUVs). To accomplish the assembly of a nucleus in GUVs, we confine interphase egg extract of *Xenopus laevis* supplemented with *Xenopus* sperm chromatin by the inverted emulsion method. We incorporate an extended waiting time as a parameter to enhance GUV yield, based on the finding that the formation of a lipid monolayer at the oil-water interface, a crucial step in the inverted emulsion method, often requires a prolonged period (*25*). Additionally, we introduce chloroform into our lipid-dispersed oil, following reported procedures that involve adding organic solvents to promote GUV formation by aggregating lipids and improving their adsorption rate at the oil-water interface (*26*). Using GUVs formed by encapsulating the interphase egg extract, we induce nuclear assembly reactions in the GUVs. To confirm nuclear reconstitution, we first identify the functionality of the nuclear membrane by a nuclear import assay. Then, we conduct molecular confirmation of the nuclear membrane by immunostaining, and quantitatively characterize the nuclear assembly events and geometric features of the formed GUVs and nuclei.

Results

Formation of GUVs encapsulating *Xenopus* egg extract

To improve the encapsulation of *Xenopus* interphase egg extract (see "Materials and Methods" for details on the preparation of *Xenopus* interphase egg extract and sperm chromatin) into GUVs by the inverted emulsion method, we assessed the impact of implemented waiting time (τ: duration of waiting time; τ = 0/60/120 min) and added chloroform (Δ: relative volume of added chloroform to the lipid-dispersed oil; Δ = 0/5/10%) in our protocol of the inverted emulsion method (Fig. 1; see "Materials and Methods" for details on the intra-GUV nuclear assembly protocol). Representative confocal micrographs of the formed GUVs are shown in Fig. 2A. At τ = 0 min and Δ = 0%, we observed that the number and size of GUVs encapsulating the egg extract were notably small, unlike the GUVs encapsulating a typical dilute aqueous solution shown in Fig. S1. Meanwhile, we found an increasing trend in the number of GUVs encapsulating the egg extract with prolonged waiting time and higher volumes of added chloroform. These observations suggest that GUV-formation via the inverted emulsion method can be enhanced by implementing prolonged waiting time and adding chloroform to lipid-dispersed oil.

To evaluate the impact of waiting time and chloroform addition, we analyzed 1) the number of GUVs, 2) encapsulation efficiency of *Xenopus* egg extract in the GUVs, and 3) GUV diameters. We found that both waiting time and chloroform volume significantly increased the number of GUVs formed, with no significant interactions between these parameters (Table S1). Pairwise comparisons highlighted the role of chloroform volume, especially between Δ = 0% vs. 10% and Δ = 5% vs. 10%, while waiting time had no clear contribution (Tables S2-3, Fig. 2B). Chloroform volume notably influenced the proportion of GUVs encapsulating GFP-dispersed egg extract, enhancing encapsulation across all Δ conditions, whereas waiting time had no significant effect (Tables S4-6, Fig. 2C). Although most GUVs were below 5 μm (Fig. 2D), both waiting time and chloroform volume significantly increased the number of GUVs larger than 5 μm, with chloroform having a more distinct effect (Tables S7-9, Fig. 2E). For the percentage of GUVs with diameters larger than 5 μm, only waiting time had a significant effect (Table S10), increasing the proportion between τ = 0 min and 120 min, while chloroform volume had no noticeable impact (Tables S11-12, Fig. 2F). Overall, these results suggest that *i*) waiting time and chloroform volume both increase the number of GUVs and the number of larger GUVs, *ii*) chloroform enhances encapsulation of the egg extract, and *iii*) waiting time increases the proportion of larger GUVs.

Formation of nucleus-like structures in GUVs

To initiate nuclear assembly reactions in GUVs encapsulating sperm chromatin-added *Xenopus* interphase egg extract, GUVs formed under various waiting time and chloroform conditions were incubated at 22ºC (or 23ºC) for 90 min. A nuclear import assay utilizing GFP fused with a nuclear localization signal derived from simian vacuolating virus 40 (GFP-NLS; see "Materials and Methods" for details on the preparation of GFP-NLS) was conducted as the primary means of identifying nucleus assembly, following established protocols in water-in-oil emulsions (*20-22*). In this assay, GFP-NLS is expected to be transported into the nucleus if a functional nuclear membrane with nuclear pore complexes is assembled on the surface as illustrated in Fig. 1C, while passive dispersion of GFP without the NLS-peptide is anticipated in the GUV lumen. Hereafter, the former

condition is denoted as "NLS(+)", and the latter as "NLS(-)". Representative micrographs of these GUVs in the top row of Fig. 3A and Fig. S2 demonstrated that GFP clearly accumulated at the same location as dense DNA in the GUVs under the NLS(+) condition, suggesting active nuclear import of GFP-NLS into the assembled nucleus. In contrast, GFP was homogeneously dispersed in the GUVs containing dense DNA under the NLS(-) condition, albeit with a slight accumulation of GFP lacking the NLS-peptide at the same location as dense DNA observed in several confocal micrographs of GUVs in NLS(-) samples (Fig. S3). These confocal micrographs indicate successful assembly of nucleus-like structures in GUVs.

Immunostaining of nuclear pore complexes on nuclear membrane

To verify the presence of a nuclear membrane on the surface of nucleus-like structures formed in GUVs (top row of Fig. 3A and Fig. S2), we conducted immunostaining of nuclear pore complexes (NPCs) using NPC antibodies (mAb414) (*27,28*). GUVs containing a nucleus-like structure were fixed with 2.0% glutaraldehyde and stained with mAb414-Alexa Fluor 594 (mAb414-AF594; see "Materials and Methods" for the details on immunostaining). Confocal micrographs of the GUVs are shown in the top row of Fig. 3B and Fig. S4. As a positive control experiment, we conducted immunostaining of nuclei formed in the bulk form of sperm chromatin-added *Xenopus* interphase egg extract using the same procedure, as depicted in the bottom row of Fig. 3B and Fig. S5. These confocal micrographs confirmed accumulations of mAb414-AF594 signals at the periphery of nucleus-like structures in the GUVs, as well as at the periphery of nuclei formed in the bulk extract. Manual inspection of the micrographs revealed that more than 15% of nucleus-like structures showed the presence of NPCs on their surfaces (28 nucleus-like structures among the 169 structures fixed, immunostained, and inspected in total). The rest of nucleus-like structures exhibited overstaining of their interior by mAb414-AF594 (Fig. S6). These immunostaining results indicate the presence of a nuclear membrane on the surfaces of a certain number of nucleus-like structures observed, thus confirming the successful reconstitution of the nucleus in the GUVs.

Quantitative characterization of nucleus-like structures in GUVs

To characterize nucleus-like structures containing DNA and GFP-NLS accumulated through nuclear import (top row of Fig. 3A and Fig. S2), we analyzed fluorescence in GUVs formed under each of NLS(+) and NLS(-) conditions and incubated for nuclear assembly reactions. We first defined C1 and C2 compartments in GUVs containing a nucleus-like structure carrying dense DNA (Fig. 4A) and extracted the mean fluorescence intensity in C1 and C2 compartments (Fig. S8). We then computed the ratio of the fluorescence intensity (Fig. 4B-C). The violin plot of SYTO 41 intensity ratio showed similar distributions and mean values of approximately 2.3 under both NLS(+) and NLS(-) conditions (see Table S13 for the result of t-test), in Fig. 4B. In contrast, the distributions of GFP intensity ratio appeared significantly different between the two conditions (p = 5.37e-68; see Table S14 for the result of t-test), with mean values of approximately 1.6 for NLS(+) and 1.2 for NLS(-), as seen in Fig. 4C. These results suggest: *i*) the presence of dense DNA in the C1 compartment, and *ii*) significantly higher accumulation of GFP-NLS in the C1 compartment under NLS(+) condition than NLS(-) condition.

To evaluate the impact of waiting time and chloroform addition on the formation of nucleus-like structures in GUVs, we quantified structures containing both dense DNA and

accumulated GFP-NLS. “Nucleus-like compartments” (NLCs) were defined as C1 compartments having significantly higher GFP intensity than C2 compartments, determined by a threshold GFP intensity ratio of ~1.5 (Fig. 4C; see “Materials and Methods” for the details on the definition and identification of NLCs). We observed successful formation of NLC-containing GUVs only under conditions where both waiting time and chloroform volume were non-zero (Fig. 4D). Among these parameters, we confirmed that only chloroform volume had a significant effect on the number of NLC-containing GUVs, with no significant interaction between the two parameters (Tables S15-17 and Fig. 4D). These results indicate that chloroform addition promotes the formation of NLCs in GUVs.

To assess the impact of the GUV size on the successful formation of NLCs and nuclei confirmed by immunostaining, we calculated the diameter of GUVs observed under the condition of $\tau = 120$ min and $\Delta = 10\%$. Statistically significant differences were observed between all combinations of GUVs containing an NLC, GUVs without NLC, and GUVs containing a nucleus as shown in Fig. 4E (see “Materials and Methods” for the details on statistical analysis and Tables S18-19 for the results). The mean diameter of GUVs containing an NLC was 6.6 μm, that of GUVs without NLC was 5.1 μm, and that of GUVs containing a nucleus was 10.2 μm as indicated with green bars in Fig. 4E. In addition, we plotted the diameters of GUVs containing an NLC (grey circles) and a nucleus (magenta triangles) against observed diameters of NLCs and the nuclei and found a positive correlation between GUV volume and NLC and nucleus volume (correlation coefficient: $\rho \sim 0.93$, power law fit result: $y = 0.086\, x^{1.18}$), as shown in Fig. 4F. The corresponding NLC-to-GUV volume ratio and nucleus-to-GUV volume ratio were approximately 0.27 for NLCs and 0.25 for nuclei, as shown in Fig. 4G (see “Materials and Methods” for the details on statistical analysis and Table S20 for the result). These results suggest three points: *i*) NLC formation and nucleus formation are more likely to occur in larger GUVs within the observed diameter range, *ii*) the size of NLCs and nuclei tends to increase with the size of GUVs within the observed volume range, and *iii*) the volume ratio between NLC and GUV and that between nucleus and GUV have similar distributions.

Discussion

In this study, we achieved the reconstitution of the cell nucleus in GUVs formed by the inverted emulsion method. Implementation of prolonged waiting time and addition of chloroform into lipid-dispersed oil improved the number of GUVs formed by the inverted emulsion method and the proportion of GUVs encapsulating sperm chromatin-added *Xenopus* interphase egg extract in the observed GUVs (Fig. 2). We found the formation of numerous nucleus-like structures in the GUVs demonstrating their nuclear import capability (Figs. 3A and S2). Moreover, we confirmed the presence of nuclear pores on their surfaces (Figs. 3B and S4), hence the presence of a nuclear membrane, by investigating through immunostaining of nuclear pore complexes. Furthermore, we identified an increase in the assembly frequency of nucleus-like compartments (NLCs), particularly along with an increase of added chloroform volume, as seen in Fig. 4D, and discovered a positive correlation between the size of GUVs and the size of internal NLCs and nuclei (Fig. 4F).

In our investigation, we noted that the implementation of waiting time and the addition of chloroform not only increased the number of GUVs encapsulating the egg extract but also enabled the formation of GUVs encapsulating a high concentration of the egg extract (Fig. S8). We hypothesize that implemented waiting time and added chloroform in lipid-dispersed oil enhance the adsorption of lipid molecules at the oil-water interface and facilitate the formation of GUVs with more stable lipid membranes by the inverted emulsion method (*25,26*). As a result, leakage of the encapsulated egg extract from the interior of the GUVs could have been reduced owing to the increased stability of the GUV membrane, while the internal solution of GUVs formed by the inverted emulsion method normally experiences dilution of the internal content (*29,30*), as demonstrated in Figs. S1 and S8. Provided that the probability of the nuclear assembly event decreases through the loss of required molecules by the extract leakage, the higher concentration of the egg extract in GUVs could have contributed to the observed increase in NLC formation (Fig. 4D).

In general, chloroform is deliberately eliminated from lipid-dispersed oil through evaporation as it is widely considered harmful to biochemical reactions embedded in GUVs (*30-32*). On the other hand, recent investigations employing the inverted emulsion method have demonstrated successful induction of gene expression reactions (*29*) and the bundle formation of cytoskeletal proteins (*33-36*) in GUVs under conditions where chloroform was deliberately added into the lipid-dispersed oil. These studies suggest that chloroform may have limited impact on biochemical reactions in GUVs, at least at the concentrations utilized in these studies. Therefore, we adopted chloroform concentrations in our lipid-dissolved oil (Δ = 5/10%) consistent with those used in previous studies, leading to the formation of the numerous egg extract-encapsulating GUVs (Fig. 2) and successful nuclear and NLC assembly in the GUVs (Figs. 3, 4D-G, S2, and S4).

The reconstitution of cell nuclei under micrometer-scale three-dimensional confinement has previously relied on water-in-oil emulsions, where the confirmation of assembled nuclei was achieved only through a nuclear import assay as shown in Fig. S9 (*20-22*). In contrast, our approach involves encapsulating the egg extract in a lipid bilayer of GUVs and reconstitutes a nucleus in the GUVs. The semi-permeability of the lipid bilayer allowed the exchange of molecules between the inside and outside of the GUVs, while essentially isolating the internal solution from the outer environment in confinement. This setup enabled the characterization of nucleus-like structures in an additional approach, similarly to previous studies of *in vitro* nuclei formed in the bulk extract. We first identified the formation of nucleus-like structures in GUVs by a nuclear import assay (Fig.

3A) and additionally conducted their molecular characterization through immunostaining (Fig. 3B). Our findings, indicating that only approximately 17% of NLCs carried nuclear pore complexes on their surfaces, highlight the significance of GUV encapsulation in providing a more comprehensive understanding of *in vitro* nuclei formed under confinement in GUVs.

We obtained several insights into size. First, we observed a significantly higher mean diameter of ~10.2 μm for GUVs containing a nucleus, as shown in Fig. 4E, compared to the mean diameter of GUVs with or without NLC. We consider that this discrepancy may be attributed to an unidentified effect of the immunostaining procedure developed in this study but not necessarily a prerequisite for nuclear assembly to occur. Furthermore, we confirmed a proportional relationship between the volume of GUVs and that of NLCs and nuclei (Fig. 4F), where the evaluated power-law exponent fitted to 1.18. This exponent is larger than the known exponents (0.7-0.9) between cell volume and nucleus volume in various natural cells (*37*), resulting in a relatively higher nuclear-to-cytoplasmic (N/C) volume ratio in these GUVs compared to many natural cells (Fig. 4G). We attribute this high N/C ratio to the large volumes of sperm chromatin encapsulated in the GUVs. Additionally, we discovered that the size range of GUVs containing an NLC and nucleus spanned approximately 1 to 16 μm, consistent with reported dimensions of GUVs encapsulating *Xenopus* egg extract of unspecified types (*24*). In contrast, we confirmed the presence of larger emulsions in the lipid-dispersed oil just before the phase transfer procedure in the inverted emulsion method (Fig. S10). These observations might be linked to instances of GUV rupture arising from the inverted emulsion method (*31,38,39*). Lastly, we found that a significant subset of the formed GUVs exhibited sizes smaller than the standard dimensions of *Xenopus laevis* sperm chromatin (approximately 10 μm along the long axis), suggesting the potential encapsulation of partial sperm chromatin fragments within the GUVs smaller than 10 μm. Considering the broader applicability of the proposed protocol, it is anticipated that the protocol could facilitate the complete encapsulation of arbitrarily long DNA molecules, including those at a genome-scale. To achieve such encapsulation, it might be necessary to investigate methods for handling long DNA molecules to prevent fragmentation due to physical forces or to develop techniques for sorting GUVs to ensure the complete encapsulation of target DNA.

Taken together, this study has enabled the reconstitution of cell nuclei in GUVs, opening a range of potential applications. Firstly, it may facilitate the investigation of the interaction between the cell cortex and nuclear assembly (*23*), which has likely been hindered by the absence of cell cortex anchoring proteins at the boundary of water-in-oil emulsions (*40*). Moreover, the established protocol holds promise for evolving into a method for transplanting artificial chromosomes into various eukaryotic cells, integrating with artificial chromosome/genome technologies (*41-44*) and GUV-cell fusion techniques (*45,46*). For chromosome transplantation, further optimization of lipid adsorption to the oil-water interface and investigation into phase transfer conditions in the inverted emulsion method might be necessary to form large GUVs encapsulating DNA of arbitrary size. Finally, we believe that the reconstituted cell nuclei in GUVs will serve as a powerful tool for constructing artificial cellular systems closely mimicking eukaryotic cells in bottom-up synthetic biology research.

Materials and Methods

Preparation of interphase egg extract and sperm chromatin of the frog *Xenopus laevis*

Interphase egg extract was prepared as described previously (*47*) with modifications as follows: to convert the cell cycle stage of the egg extract from mitosis into interphase, unfertilized eggs were crushed using KMH (100 mM KCl, 2.5 mM $MgCl_2$, 20 mM HEPES-KOH at pH 7.7) containing 1 mM $CaCl_2$ rather than a calcium-ionophore treatment; to completely separate the egg extract from insoluble material (*e.g.*, actin filaments and mitochondria), crude egg extract isolated by the initial centrifugation was diluted in KMH (10% volume of the original extract), and then clarified by another round of centrifugation at 45,000×*g*. Sperm chromatin was prepared as described previously (*47*). In every preparation of the egg extract and sperm chromatin, their quality was evaluated by monitoring nuclear assembly in the bulk format (bottom row of Fig. 3B and Fig. S5) and in water-in-oil emulsions (Fig. S9) under a fluorescence microscope.

Preparation of GFP-NLS

GFP-NLS in Figs. 3B, 4B NLS(+), 4C, 4E w/ nucleus, 4F Nuclei, S1, S4-6, S10 was prepared by following a standard protocol (*48*). GFP-NLS used in other sections of this paper was prepared by Dr. Yuki Hara by following a similar standard protocol. Briefly, *Escherichia coli* BL21 (DE3) cells were transformed with a pGEX vector containing a GFP-NLS gene. The cells were incubated in four 250 mL aliquots of LB medium at 30°C with shaking at 250 RPM until OD_{600} ~ 0.8. 1 mM IPTG was added, and the cultures were further incubated for 5 h. The cells were harvested by centrifugation, and the pellets were stored at -80°C until next day. On the following day, the frozen cell pellets were resuspended in PBS lysis buffer (consisting of PBS pH 7.2 and 1% Triton X-100) and lysed by gentle sonication. Then, the lysate was centrifuged at 12,000×*g*, 4°C for 15 min. The supernatant was collected and mixed with a 50:50 slurry of glutathione-Sepharose beads in chilled PBS lysis buffer. The bead-cell mix was incubated at 4°C to trap proteins on the beads. Then, the beads were washed with ice-cold PBS containing protease inhibitors and loaded into a disposable chromatography column. Trapped GST-GFP-NLS was eluted with ice-cold 50 mM Tris-HCl (pH 8.0) containing 20 mM reduced glutathione. Molecular weight of the collected GST-GFP-NLS was confirmed by polyacrylamide gel electrophoresis. Throughout this study, GST-GFP-NLS is referred to as "GFP-NLS".

Intra-GUV nuclear assembly protocol

To achieve reconstitution of cell nuclei in GUVs, we designed an experimental protocol as illustrated in Fig. 1. Briefly, the protocol consists of three steps: 1) preparation of *Xenopus* interphase egg extract supplemented with sperm chromatin, 2) formation of GUVs encapsulating the sperm chromatin-added interphase egg extract by the inverted emulsion method, and 3) induction of nuclear assembly reactions in the formed GUVs. In the first step, the sperm chromatin-added egg extract was prepared for *in vitro* nuclear assembly reactions (*15-17*) as depicted in Fig. 1A. In the second step, GUVs encapsulating the egg extract were formed at a chilled temperature by the inverted emulsion method (*25*) with two modifications to the conventional protocol: *i*) implementing prolonged waiting time and *ii*) adding chloroform into lipid-dispersed oil to facilitate the formation of GUVs encapsulating the egg extract as illustrated in Fig. 1B. In the third step, the GUVs were incubated at 22-23ºC to initiate the assembly of interphase nuclei within them as depicted in Fig. 1C.

352 **Formation of GUVs encapsulating *Xenopus* interphase egg extract**
353 The lipid-dispersed oil (lipid-oil) was prepared using the following procedure. 1-
354 palmitoyl-2-oleoyl-glycero-3-phosphocholine (POPC) at a concentration of 25 mg mL^{-1} in
355 chloroform, and 1,2-dioleoyl-sn-glycero-3-phosphoethanolamine-N-(lissamine rhodamine
356 B sulfonyl) ammonium salt (RhPE) at 1 mg mL^{-1} in chloroform, both purchased from
357 Avanti Polar Lipids (USA), were taken to a disposable glass bottle with a screw top
358 (Laboran, As One, Japan). The chloroform was evaporated in a desiccator for 30-60 min
359 using a vacuum pump. Mineral oil (M5904, Sigma Aldrich) was then immediately added
360 to the bottle. The final composition of the lipid-oil was 2.5 mM of POPC with 0.1% (mole
361 percent) RhPE in mineral oil. For the GUVs in immunostaining experiment, RhPE was not
362 added. Subsequently, chloroform (Δ = 0/5/10% depending on the experimental condition)
363 was added using a disposable pipette. The screw top was tightly closed, and a strip of
364 adhesive tape was attached to ensure sealing. The lipid-oil was sonicated at 60°C for 1 h
365 and stored at room temperature until use. In all experiments, the lipid-oil was consumed
366 within a week after preparation. The lipid-oil was sonicated at 60°C for 1 h before each
367 use.

368 GUVs were formed by the inverted emulsion method (*25*) according to the following
369 protocol. First, two 1.5 mL disposable tubes and a 2.0 mL disposable centrifuge tube were
370 prepared. 150 µL of egg lysis buffer (250 mM sucrose, 10 mM HEPES-KOH pH 7.7, 50
371 mM KCl, 2.5 mM $MgCl_2$, and 1 mM dithiothreitol) (*49*) was added to each of the 1.5 mL
372 tubes, and 1.0 mL of lipid-oil was added to the 2.0 mL centrifuge tube. All tubes were
373 then placed on ice. Next, 25 µL of frozen *Xenopus* interphase egg extract stored at -80°C
374 was thawed on ice. Subsequently, 0.5 µL of energy mix (50 mM ATP, 50 mM $MgCl_2$, 10
375 mM phosphocreatine, 100 µg mL^{-1} creatine kinase, pH 7.5 adjusted with NaOH) and 0.5
376 µL of GFP-NLS (3.4 mg mL^{-1} for experiments in Figs. 2, 3A top, 4D, 4E w/ and w/o
377 NLC, 4F-G NLCs, S2, S8-9, S11-12 and 11.1 mg mL^{-1} for experiments in Figs. 3B, 4B
378 NLS(+), 4C, 4E w/ nucleus, 4F Nuclei, 4G Nuclei, S1, S4-6, S7 NLS(+), S10) for NLS(+)
379 condition or GFP (7.7 mg mL^{-1} for experiments in Figs. 3A bottom, 4B-C NLS(-), S3, S7
380 NLS(-); purchased from Chromotek, Germany) for NLS(-) condition were added to the
381 thawed egg extract. This mixture was briefly vortexed and spun down. Subsequently, 0.5
382 µL of thawed *Xenopus* sperm chromatin was added on ice and the extract was mixed by
383 gently pipetting four times. 25 µL of this extract mix was then added to 1 mL of chilled
384 lipid-oil in the 2.0 mL centrifuge tube. Additionally, 150 µL of lipid-oil was layered on
385 top of the egg lysis buffer in the two 1.5 mL tubes on ice. These three tubes were
386 incubated on ice for the designated duration of waiting time (τ = 0/60/120 min).

387 Following the incubation of the oil-water interface on ice, the mixture of lipid-oil and the
388 egg extract was vortexed for 1 min at 3,200 RPM using a Vortex-Genie 2 (Scientific
389 Industries, Inc.). 500 µL of the vortexed mixture of the egg extract in lipid-oil was
390 immediately layered on top of each of the chilled lipid-oil layers in the 1.5 mL tubes. The
391 two 1.5 mL tubes were centrifuged at 9,000×*g*, 4°C for 30 min. During this centrifugation,
392 a new 1.5 mL tube filled with 1 mL of the egg lysis buffer was prepared and chilled on
393 ice. Subsequently, the centrifuged tubes were collected, and the formed GUVs in the
394 bottom pellet were transferred into 1 mL of the chilled egg lysis buffer in a 1.5 mL tube by
395 piercing the side wall of the pellet in the tube with a syringe needle and applying air
396 pressure from the open top of the tube using an index finger. Finally, the collected GUVs
397 dispersed in the egg lysis buffer were vortexed briefly and kept on ice until further
398 experiment.
399

Induction of nuclear assembly reactions

Nuclear assembly in GUVs encapsulating sperm chromatin-added *Xenopus* interphase egg extract was conducted by incubating the formed GUVs dispersed in the egg lysis buffer either on a tube rack at 23°C or on a block incubator set at 22°C for 90 min. Note that all GUVs encapsulating the egg extract formed by our inverted emulsion method were incubated for nuclear assembly reactions before fluorescence staining and microscopy.

Nuclear assembly under bulk condition was performed by the following procedure. Firstly, the frozen egg extract, energy mix, GFP-NLS, and sperm chromatin were thawed on ice. Subsequently, 1 μL of energy mix and 1 μL of GFP-NLS were added to 50 μL of the thawed egg extract in a 0.5 mL tube. This egg extract was vortexed briefly, spun down, and placed on ice immediately. Then, 1 μL of sperm chromatin was added to the egg extract. This egg extract was gently pipetted four times, spun down briefly, and placed back on ice immediately. The 0.5 mL tube containing the extract mix was then placed on a block incubator set at 22°C and incubated for 90 min to induce nuclear assembly reactions in the bulk egg extract.

Fluorescence staining and preparation of glass slide samples for microscopy

GUVs encapsulating the egg extract dispersed in the egg lysis buffer were centrifuged at 200×*g* for 5 min at room temperature. The supernatant was carefully removed, and the sample volume was reduced to 140 μL. For fluorescence staining of DNA, 0.14 μL of 5 mM SYTO 41 (Thermo Fisher Scientific) was added to the sample by a 1,000× dilution. Subsequently, the stained GUVs were briefly vortexed and transferred into the open well of a Frame-Seal chamber (SLF1201, Bio-Rad) attached to a BSA-coated glass slide. The chamber was immediately sealed with a No.1 glass coverslip coated with BSA. To facilitate microscopy, the glass slide sample was immediately inverted so that the No.1 coverslip faced downward, allowing the GUVs to settle towards the bottom surface prior to microscopy.

Microscopy

An inverted microscope (IX71, Olympus) equipped with an oil immersion objective (PlanApoN 60×, 1.45 NA, Olympus), fluorescence filters (460/80 nm, 520/35 nm, and 617/73 nm Bright-Line single-bandpass filters, Semrock, USA), a laser combiner (405/488/561 nm, ALC5000, Andor Technology, UK), a spinning disk confocal unit (CSU-X1, Yokogawa, Japan), and an EM-CCD camera (iXon X3, Andor Technology, UK) was used for all micrographs in the main text of this paper. Imaging sequences were programmed and executed using iQ2 software (Andor Technology, UK).

Immunostaining of nuclear pore complexes on nuclear membranes

Immunostaining of nuclear pore complexes (NPCs) on the nuclei formed in the bulk form of the egg extract and in GUVs encapsulating the egg extract was conducted as follows.

For fixing nuclei formed in bulk form of the egg extract, 50 μL of the nuclei-containing egg extract was first mixed with 150 μL of the egg lysis buffer and pipetted gently. 200 μL of fixation solution (4% glutaraldehyde in 80 mM KCl and 10 mM Tris-HCl pH 7.7) was added, and the tube was immediately placed on ice and incubated for 1 h. After the incubation, the fixed nuclei were transferred to a 1.5 mL tube filled with 1 mL of quenching solution (10 mM Tris-HCl pH 7.7, 250 mM sucrose, 50 mM KCl, 1% BSA) on ice. The sample was centrifuged at 200×*g*, 4°C for 5 min, and the supernatant was gently removed. The sample was then centrifuged again, and the supernatant was removed down

450 to 100 μL. To stain NPCs on the membrane of the fixed nuclei, 1 μL of 0.5 mg mL^{-1}
451 mAb414-AF594 was added and gently mixed by pipetting. The fixed nuclei with
452 mAb414-AF594 were incubated on ice overnight. On the next day, the sample was
453 centrifuged at 200×*g*, 4°C for 5 min. The supernatant was removed down to 100 μL, and
454 0.1 μL of 5 mM SYTO 41 was added for DNA staining. The entire volume of the
455 immunostained nuclei was enclosed in a Frame-Seal chamber between a No.1 glass
456 coverslip and a glass slide, both of which were coated with BSA.
457
458 The fixation of nuclei formed in GUVs encapsulating the egg extract was performed in the
459 following procedure. The GUVs were centrifuged at 200×*g*, 4ºC for 5 min, and the
460 supernatant was removed down to 100 μL. The tube containing the GUVs was placed on
461 ice, and 100 μL of the fixation solution was added. After 1 h of incubation on ice, the
462 fixed GUVs were mixed with 1 mL of quenching solution and centrifuged at 1,000×*g* for
463 5 min at 4ºC. The supernatant was removed, and the volume was reduced to 100 μL. The
464 quenching and washing of the fixed GUVs were repeated once, and the sample volume
465 was adjusted to 100 μL. The fixed GUVs with NPC-antibodies were then incubated on ice
466 overnight. The following day, 1 mL of quenching solution was added, the sample was
467 centrifuged at 1,000×*g*, 4ºC for 5 min, and the supernatant was reduced down to 100 μL.
468 0.1 μL of 5 mM SYTO 41 was added for DNA staining, and the immunostained GUVs
469 were enclosed in a Frame-Seal chamber between a No.1 glass coverslip and a glass slide,
470 both of which were coated with BSA.
471
472 **Image segmentation of GUVs**
473 Image segmentation of GUVs on acquired micrographs was performed using *cellpose 2.0*
474 (*50,51*) implemented in Python. The envelopes of GUVs were primarily segmented using
475 a built-in model ("CP"), and the quality of the segments was manually inspected and
476 corrected on the graphical user interface (GUI) of *cellpose 2.0*.
477
478 **Number, internal GFP intensity, and diameter of GUVs**
479 The analysis of GUV fluorescence using above generated segment masks was performed
480 in MATLAB. The number of GUVs was determined by computing the number of
481 segments. The mean GFP intensity in the GUVs, denoted as I_{GFP}, was computed by
482 extracting intensity values in the GFP channel using the segmentation mask and taking
483 their mean. The diameter of the GUVs was defined as the reduced diameter of each circle
484 having a corresponding area of individual segments. To determine the mean GFP intensity
485 in the background of each micrograph, three arbitrary rectangular regions with at least
486 1,056 pixels were carefully selected in the background of each micrograph. The
487 corresponding mean GFP fluorescence intensity was computed for each rectangular
488 region, and the average of the three means was calculated. The threshold of GFP
489 encapsulation (dashed lines in Fig. S8) was defined by mean + 3SD of the mean GFP
490 intensity in each background.
491
492 **Exclusion of GUVs containing aggregated GFP**
493 GUVs containing aggregated GFP were manually excluded from the dataset used to
494 compute the proportion of GUVs encapsulating the GFP-dispersed egg extract in the
495 observed GUVs (Fig. 2C). This exclusion aimed to mitigate artifacts in the computed
496 proportion arising from GFP aggregation in three-dimensional space. This issue was
497 observed in all micrographs acquired after completing the entire protocol of nuclear
498 assembly in GUVs (Fig. 1). Since the GUVs in the micrographs of Fig. 2 had already
499 undergone 23ºC incubation for nuclear assembly reactions, several GUVs in the acquired

micrographs exhibited positive indications of nuclear import by GFP-NLS within them. Theoretically, the mean GFP intensity computed from a confocal micrograph of such GUVs with aggregated GFP always yielded a higher mean GFP intensity than a confocal micrograph of GUVs without GFP aggregation even if the same amount of GFP was encapsulated. Consequently, the mean GFP intensity of the GUVs containing the aggregation did not precisely reflect the concentration of GFP encapsulated in the GUV. Because the purpose of the analysis in Fig. 2C was to evaluate GFP encapsulation in the GUVs, we considered the inclusion of data from GUVs carrying such aggregated GFP inadequate and excluded the GUVs from this specific analysis in Fig. 2C. The same parameter computed from data including the GUVs containing aggregated GFP is shown in Fig. S11. Additionally, raw GFP intensity values in the GUV lumen and the background of these GUVs are plotted in Fig. S12. Comparisons between plots excluding the GUVs containing aggregated GFP (Figs. 2C and S8) and those including them (Figs. S11-12) indicate only minor changes.

Definition and identification of NLCs in GUVs

To differentiate between C1 compartments (Fig. 4A) containing a significantly high level of GFP-NLS from those with a lower level, we set a threshold for the GFP intensity ratio, as indicated by the dashed line in Fig. 4C. This threshold was determined as the mean + 3SD of the GFP intensity ratio under NLS(-) conditions (dashed line in Fig. 4C). We used this threshold to interpret accumulation of GFP-NLS in C1 compartment: if the ratio exceeded the threshold, it indicated GFP-NLS accumulation. Utilizing this threshold, we defined a "nucleus-like compartment" (NLC) as a C1 compartment with a GFP intensity ratio higher than the threshold.

To identify NLCs in GUVs, GUVs containing dense DNA (C1 compartment in Fig. 4A) were initially identified in micrographs through manual inspection. Subsequently, the envelopes of the GUVs and their internal C1 compartments were manually segmented in RhPE and SYTO41 channels using the interactive *drawfreehand* function in MATLAB. Mean intensity values of SYTO 41 signals in the C1 and C2 compartments were then computed using the segment masks. Similarly, mean GFP intensities in the C1 and C2 compartments were computed using the same segment masks. Next, the ratio of mean intensities in the C1 and C2 compartments was computed for both the SYTO 41 and GFP channels. The threshold for the GFP intensity ratio was determined based on the above definition (computed threshold: ~1.5). Furthermore, to ensure the encapsulation of DNA and GFP-NLS in the NLCs, the mean fluorescence intensity of both SYTO 41 and GFP in the background (Fig. S7) was calculated. This computation was done by extracting three arbitrary rectangular regions from the background, each containing at least 1,517 pixels. The mean fluorescence intensity of each region was computed, and the average of these three mean values was taken.

Number and size of GUVs containing an NLC

The number of GUVs containing an NLC was determined by manually inspecting all confocal micrographs of GUVs encapsulating the egg extract after 90 minutes of incubation at 22°C. GUVs carrying dense DNA (C1 compartment) were manually identified, and each C1 compartment was evaluated to determine whether it contained an NLC, following the established definition. The diameters of GUVs containing an NLC and those not containing an NLC at $\tau = 120$ minutes and $\Delta = 10\%$, as shown in Fig. 4E, were computed using the following procedure. Accurate manual image segmentation of GUVs containing an NLC was conducted when all NLCs were identified. The same number of segments from GUVs without an NLC were randomly selected from the

micrographs. Using the segments of these GUVs, the reduced diameter was computed from their segment area. The volumes of GUVs containing an NLC and nucleus, as well as the volumes of the corresponding NLC and nucleus, were computed from the segment area by calculating the reduced radius and then the corresponding reduced volume as a sphere.

Statistical analysis

In the statistical analyses depicted in Figs. 2B-C, 2E, 2F, 4D, and S11, we conducted a two-way ANOVA followed by *post-hoc* Tukey's HSD tests, focusing either on the duration of waiting time or the added volume of chloroform. For the statistical analyses in Figs. 4B-C, we performed a two-sample t-test. For the statistical analysis in Fig. 4E, we used the Kruskal-Wallis test followed by a *post-hoc* Mann-Whitney U test with Bonferroni's correction. In the statistical analysis shown in Fig. 4G, we employed the Wilcoxon rank-sum test. For all analyses, resultant p-values were rounded to the first significant digit and annotated using the conventional method: "n.s." (not significant) for $p > 0.05$, "*" for $p \leq 0.05$, "**" for $p \leq 0.01$, and "***" for $p \leq 0.001$. The results of all statistical analyses are summarized in Tables S1-23.

References

(1) H. Jia, P. Schwille, Bottom-up synthetic biology: reconstitution in space and time. *Current opinion in biotechnology* **60,** 179-187 (2019).

(2) F. C. Simmel, Synthetic organelles. *Emerging Topics in Life Sciences* **3**(5), 587-595 (2019).

(3) B. C. Buddingh', J. C. van Hest, Artificial cells: synthetic compartments with life-like functionality and adaptivity. *Accounts of chemical research* **50**(4), 769-777 (2017).

(4) N. J. Gaut, K. P. Adamala, Reconstituting natural cell elements in synthetic cells. *Advanced Biology* **5**(3), 2000188 (2021).

(5) Y. Elani, Interfacing living and synthetic cells as an emerging frontier in synthetic biology. *Angewandte Chemie* **133**(11), 5662-5671 (2021).

(6) K. Y. Lee, S. J. Park, K. A. Lee, S. H. Kim, H. Kim, Y. Meroz, L. Mahadevan, K. H. Jung, T. K. Ahn, K. K. Parker, K. Shin, Photosynthetic artificial organelles sustain and control ATP-dependent reactions in a protocellular system. *Nature biotechnology* **36**(6), 530-535 (2018).

(7) S. Berhanu, T. Ueda, Y. Kuruma, Artificial photosynthetic cell producing energy for protein synthesis. *Nature communications* **10**(1), 1325 (2019).

(8) B. P. Kumar, J. Fothergill, J. Bretherton, L. Tian, A. J. Patil, S. A. Davis, S. Mann, Chloroplast-containing coacervate micro-droplets as a step towards photosynthetically active membrane-free protocells. *Chemical communications* **54**(29), 3594-3597 (2018).

(9) L. Otrin, N. Marušič, C. Bednarz, T. Vidakovic-Koch, I. Lieberwirth, K. Landfester, K. Sundmacher, Toward artificial mitochondrion: mimicking oxidative phosphorylation in polymer and hybrid membranes. *Nano letters* **17**(11), 6816-6821 (2017).

(10) N. Marušič, L. Otrin, Z. Zhao, R. B. Lira, F. L. Kyrilis, F. Hamdi, P. L. Kastritis, T. Vidaković-Koch, I. Ivanov, K. Sundmacher, R. Dimova, Constructing artificial respiratory chain in polymer compartments: Insights into the interplay between bo_3 oxidase and the membrane. *Proceedings of the National Academy of Sciences* **117**(26), 15006-15017 (2020).

(11) I. N. Westensee, E. Brodszkij, X. Qian, T. F. Marcelino, K. Lefkimmiatis, B. Städler, Mitochondria encapsulation in hydrogel-based artificial cells as ATP producing subunits. *Small* **17**(24), 2007959 (2021).

(12) N. N. Deng, M. Yelleswarapu, L. Zheng, W. T. Huck, Microfluidic assembly of monodisperse vesosomes as artificial cell models. *Journal of the American Chemical Society* **139**(2), 587-590 (2017).

(13) L. Aufinger, F. C. Simmel, Artificial gel-based organelles for spatial organization of cell-free gene expression reactions. *Angewandte Chemie International Edition* **57**(52), 17245-17248 (2018).

(14) K. Göpfrich, I. Platzman, J. P. Spatz, Mastering complexity: towards bottom-up construction of multifunctional eukaryotic synthetic cells. *Trends in biotechnology* **36**(9), 938-951 (2018).

(15) M. J. Lohka, Y. Masui, Formation *in vitro* of sperm pronuclei and mitotic chromosomes induced by amphibian ooplasmic components. *Science* **220**(4598), 719-721 (1983).

(16) D. D. Newmeyer, J. M. Lucocq, T. R. Bürglin, E. M. De Robertis, Assembly *in vitro* of nuclei active in nuclear protein transport: ATP is required for nucleoplasmin accumulation. *The EMBO journal* **5**(3), 501-510 (1986).

(17) J. Newport, Nuclear reconstitution *in vitro*: stages of assembly around protein-free DNA. *Cell* **48**(2), 205-217 (1987).

616 *(18)* Y. Hara, C. A. Merten, Dynein-based accumulation of membranes regulates
617 nuclear expansion in *Xenopus laevis* egg extracts. *Developmental cell* **33**(5), 562-575
618 (2015).
619 *(19)* J. Bisht, P. LeValley, B. Noren, R. McBride, P. Kharkar, A. Kloxin, J. Gatlin, J.
620 Oakey, Light-inducible activation of cell cycle progression in *Xenopus* egg extracts under
621 microfluidic confinement. *Lab on a Chip* **19**(20), 3499-3511 (2019).
622 *(20)* M. C. Good, Encapsulation of *Xenopus* egg and embryo extract spindle assembly
623 reactions in synthetic cell-like compartments with tunable size. *The Mitotic Spindle:*
624 *Methods and Protocols* 87-108 (2016).
625 *(21)* Y. Guan, Z. Li, S. Wang, P. M. Barnes, X. Liu, H. Xu, M. Jin, A. P. Liu, Q. Yang,
626 A robust and tunable mitotic oscillator in artificial cells. *Elife* **7**, e33549 (2018).
627 *(22)* Y. Guan, S. Wang, M. Jin, H. Xu, Q. Yang, Reconstitution of cell-cycle
628 oscillations in microemulsions of cell-free *Xenopus* egg extracts. *JoVE (Journal of*
629 *Visualized Experiments)* (**139**), e58240 (2018).
630 *(23)* J. G. Bermudez, H. Chen, L. C. Einstein, M. C. Good, Probing the biology of cell
631 boundary conditions through confinement of *Xenopus* cell-free cytoplasmic extracts.
632 *genesis* **55**(1-2), e23013 (2017).
633 *(24)* M. Chiba, M. Miyazaki, S. I. Ishiwata, Quantitative analysis of the lamellarity of
634 giant liposomes prepared by the inverted emulsion method. *Biophysical journal*, **107**(2),
635 346-354 (2014).
636 *(25)* S. Pautot, B. J. Frisken, D. A. Weitz, Production of unilamellar vesicles using an
637 inverted emulsion. *Langmuir* **19**(7), 2870-2879 (2003).
638 *(26)* C. Claudet, M. In, G. Massiera, Method to disperse lipids as aggregates in oil for
639 bilayers production. *The European Physical Journal E* **39**, 1-6 (2016).
640 *(27)* M. R. Dilsaver, P. Chen, T. A. Thompson, T. Reusser, R. N. Mukherjee, J. Oakey,
641 D. L. Levy, Emerin induces nuclear breakage in *Xenopus* extract and early embryos.
642 *Molecular Biology of the Cell* **29**(26), 3155-3167 (2018).
643 *(28)* M. S. Nord, C. Bernis, S. Carmona, D. C. Garland, A. Travesa, D. J. Forbes,
644 Exportins can inhibit major mitotic assembly events *in vitro*: membrane fusion, nuclear
645 pore formation, and spindle assembly. *Nucleus* **11**(1), 178-193 (2020).
646 *(29)* L. Van de Cauter, F. Fanalista, L. Van Buren, N. De Franceschi, E. Godino, S.
647 Bouw, C. Danelon, C. Dekker, G. H. Koenderink, K. A. Ganzinger, Optimized cDICE for
648 efficient reconstitution of biological systems in giant unilamellar vesicles. *ACS Synthetic*
649 *Biology* **10**(7), 1690-1702 (2021).
650 *(30)* Y. Shimane, Y. Kuruma, Rapid and facile preparation of giant vesicles by the
651 droplet transfer method for artificial cell construction. *Frontiers in Bioengineering and*
652 *Biotechnology* **10**, 873854 (2022).
653 *(31)* K. Nishimura, T. Matsuura, K. Nishimura, T. Sunami, H. Suzuki, T. Yomo, Cell-
654 free protein synthesis inside giant unilamellar vesicles analyzed by flow cytometry.
655 *Langmuir* **28**(22), 8426-8432 (2012).
656 *(32)* M. Walczak, R. A. Brady, L. Mancini, C. Contini, R. Rubio-Sánchez, W. T.
657 Kaufhold, P. Cicuta, L. Di Michele, Responsive core-shell DNA particles trigger lipid-
658 membrane disruption and bacteria entrapment. *Nature Communications* **12**(1), 4743
659 (2021).
660 *(33)* E. Loiseau, J. A. Schneider, F. C. Keber, C. Pelzl, G. Massiera, G. Salbreux, A. R.
661 Bausch, Shape remodeling and blebbing of active cytoskeletal vesicles. *Science Advances*
662 **2**(4), e1500465 (2016).
663 *(34)* T. Litschel, B. Ramm, R. Maas, M. Heymann, P. Schwille, Beating vesicles:
664 encapsulated protein oscillations cause dynamic membrane deformations. *Angewandte*
665 *Chemie International Edition* **57**(50), 16286-16290 (2018).

666 *(35)* T. Litschel, C. F. Kelley, D. Holz, M. Adeli Koudehi, S. K. Vogel, L. Burbaum, N.
667 Mizuno, D. Vavylonis, P. Schwille, Reconstitution of contractile actomyosin rings in
668 vesicles. *Nature communications* **12**(1), 2254 (2021).
669 *(36)* L. Baldauf, F. Frey, M. A. Perez, T. Idema, G. H. Koenderink, Branched actin
670 cortices reconstituted in vesicles sense membrane curvature. *Biophysical journal* **122**(11),
671 2311-2324 (2023).
672 *(37)* Y. Hara, Specialization of nuclear membrane in eukaryotes. *Journal of Cell*
673 *Science* **133**(12), jcs241869 (2020).
674 *(38)* N. Yandrapalli, T. Seemann, T. Robinson, On-chip inverted emulsion method for
675 fast giant vesicle production, handling, and analysis. *Micromachines* **11**(3), 285 (2020).
676 *(39)* A. Moga, N. Yandrapalli, R. Dimova, T. Robinson, Optimization of the inverted
677 emulsion method for high-yield production of biomimetic giant unilamellar vesicles.
678 *ChemBioChem* **20**(20), 2674-2682 (2019).
679 *(40)* R. Sakamoto, M. Tanabe, T. Hiraiwa, K. Suzuki, S. I. Ishiwata, Y. T. Maeda, M.
680 Miyazaki, Tug-of-war between actomyosin-driven antagonistic forces determines the
681 positioning symmetry in cell-sized confinement. *Nature communications* **11**(1), 3063
682 (2020).
683 *(41)* A. W. Murray, J. W. Szostak, Construction of artificial chromosomes in yeast.
684 *Nature* **305**(5931), 189-193 (1983).
685 *(42)* J. J. Harrington, G. V. Bokkelen, R. W. Mays, K. Gustashaw, H. F. Willard,
686 Formation of *de novo* centromeres and construction of first-generation human artificial
687 microchromosomes. *Nature genetics* **15**(4), 345-355 (1997).
688 *(43)* D. G. Gibson, G. A. Benders, C. Andrews-Pfannkoch, E. A. Denisova, H. Baden-
689 Tillson, J. Zaveri, T. B. Stockwell, A. Brownley, D. W. Thomas, M. A. Algire, C.
690 Merryman, L. Young, V. N. Noskov, J. I. Glass, J. C. Venter, C. A. Hutchison III, H. O.
691 Smith, Complete chemical synthesis, assembly, and cloning of a *Mycoplasma genitalium*
692 genome. *Science* **319**(5867), 1215-1220 (2008).
693 *(44)* C. A. Hutchison III, R. Y. Chuang, V. N. Noskov, N. Assad-Garcia, T. J.
694 Deerinck, M. H. Ellisman, J. F. Pelletier, Z. Qi, R. A. Richter, E. A. Strychalski, L. Sun,
695 Y. Suzuki, B. Tsvetanova, K. S. Wise, H. O. Smith, J. I. Glass, C. Merryman, D. G.
696 Gibson, J. C. Venter, Design and synthesis of a minimal bacterial genome. *Science*
697 **351**(6280), aad6253 (2016).
698 *(45)* A. C. Saito, T. Ogura, K. Fujiwara, S. Murata, S. I. M. Nomura, Introducing
699 micrometer-sized artificial objects into live cells: A method for cell–giant unilamellar
700 vesicle electrofusion. *PLoS One* **9**(9), e106853 (2014).
701 *(46)* S. Takamori, P. Cicuta, S. Takeuchi, L. Di Michele, DNA-assisted selective
702 electrofusion (DASE) of *Escherichia coli* and giant lipid vesicles. *Nanoscale* **14**(38),
703 14255-14267 (2022).
704 *(47)* K. Shintomi, T. Hirano, A sister chromatid cohesion assay using *Xenopus* egg
705 extracts. *Methods in Molecular Biology* **1515**, 3-21 (2017).
706 *(48)* M. B. Einarson, E. N. Pugacheva, J. R. Orlinick, Preparation of GST fusion
707 proteins. *Cold Spring Harbor Protocols* 2007(4), pdb-prot4738 (2007).
708 *(49)* X. Cheng, J. E. Ferrell Jr, Spontaneous emergence of cell-like organization in
709 *Xenopus* egg extracts. *Science* **366**(6465), 631-637 (2019).
710 *(50)* C. Stringer, T. Wang, M. Michaelos, M. Pachitariu, Cellpose: a generalist
711 algorithm for cellular segmentation. *Nature methods* **18**(1), 100-106 (2021).
712 *(51)* M. Pachitariu, C. Stringer, Cellpose 2.0: how to train your own model. *Nature*
713 *methods* **19**(12), 1634-1641 (2022).

Acknowledgments

We thank Dr Yuki Hara for kindly offering purified GFP-NLS and the corresponding plasmid.

Funding:
This work was supported by JST CREST JPMJCR18S5 (STakeuchi and MO), JSPS KAKENHI JP22K15080 (STakamori), JSPS KAKENHI JP19H05755 (KS), and JSPS KAKENHI JP22H02551 (KS).

Author contributions:
Conceptualization: ST1(STakeuchi), MO, ST2(STakamori)
Methodology: ST1, MO, KS, TO, ST2, HM, TK, MS
Investigation: KS, ST2, MS
Visualization: ST2
Supervision: ST1, MO, KS, TO, HM, TK, MS
Writing—original draft: ST2
Writing—review & editing: ST1, MO, KS, TO, ST2, HM, TK, MS

Competing interests: The authors declare that they have no competing interests.

Data and materials availability: All data needed to evaluate the conclusions in the paper are available in the main text or the Supplementary Materials.

Figures and Tables

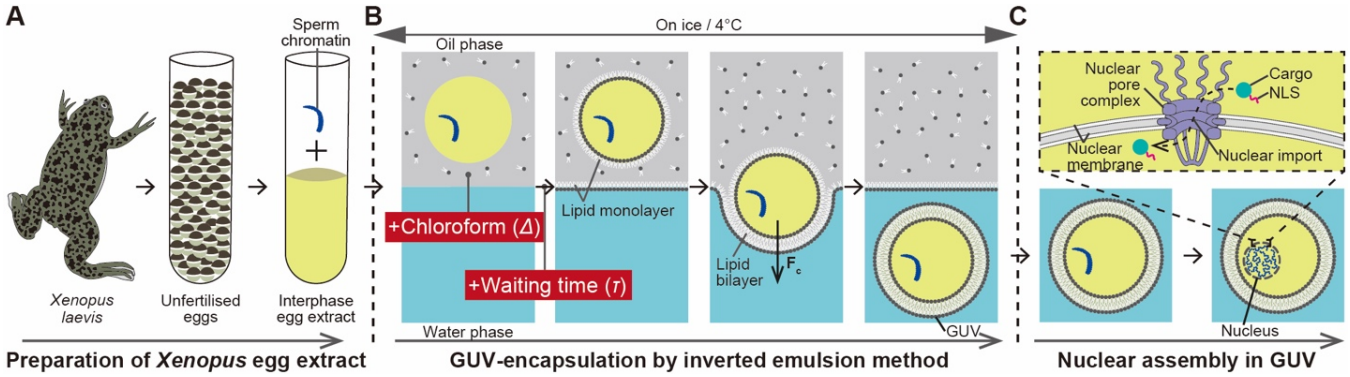

Fig. 1. Three-step protocol for the assembly of a cell nucleus in GUVs.
(**A**) Preparation of *Xenopus* interphase egg extract. Sperm chromatin is added to the egg extract prior to encapsulation into GUVs. (**B**) Encapsulation of sperm chromatin-added interphase egg extract into GUVs by the inverted emulsion method. Lipid monolayers are formed at the interfaces between water and oil phases. The formation of a lipid monolayer at the interfaces is enhanced by incubating the interfaces for the duration of the waiting time (τ) and adding chloroform in a volume (Δ) into lipid-dispersed oil. Centrifugal force (F_c) allows the egg extract emulsions surrounded by a lipid monolayer to pass through a lipid monolayer formed at the interface between the oil phase and the outside water phase, transforming them into GUVs. (**C**) Induction of nuclear assembly reactions in GUVs by incubation at 22/23°C for 90 min.

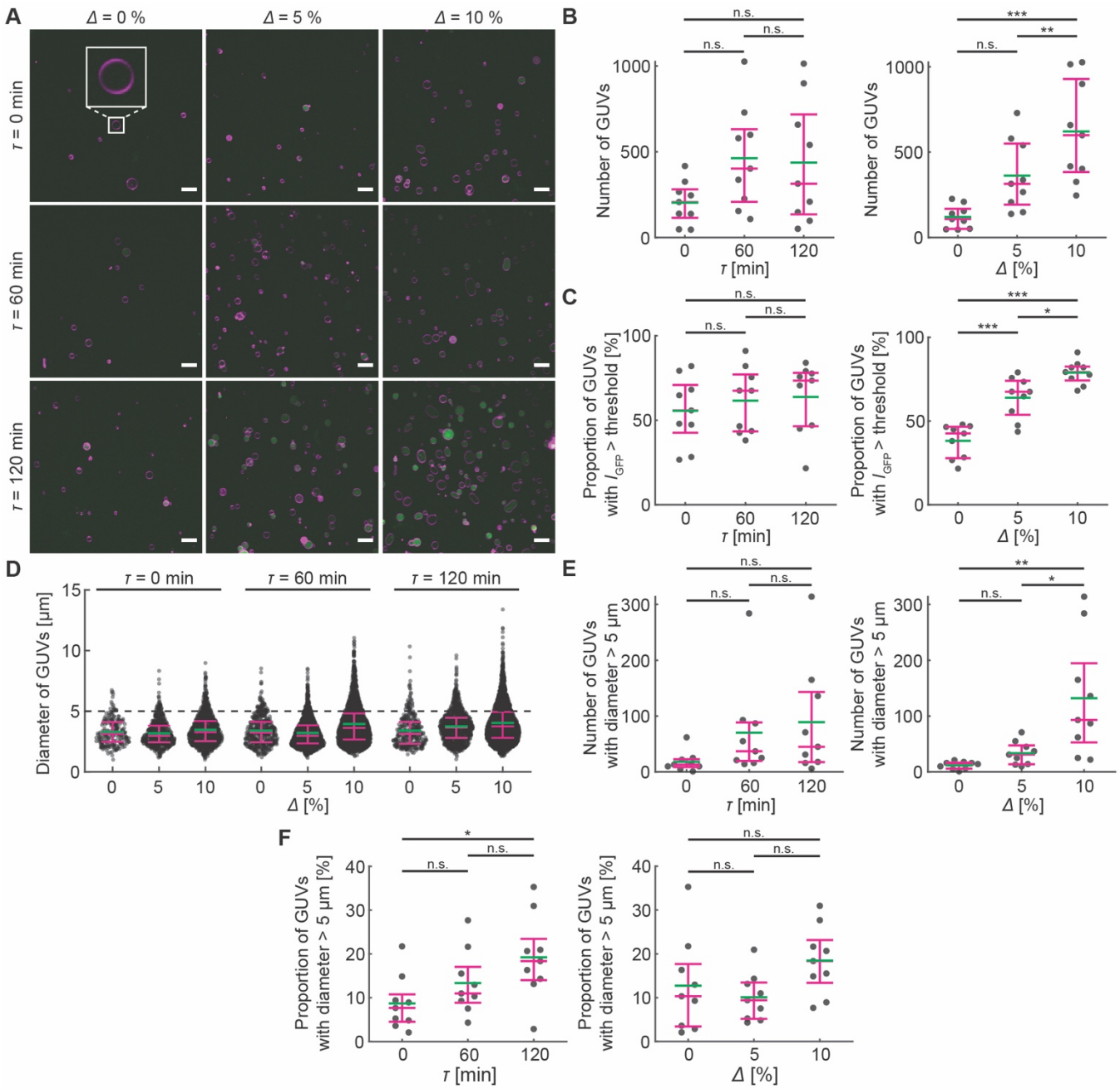

Fig. 2. Formation of GUVs encapsulating *Xenopus* interphase egg extract. (**A**) Representative micrographs of GUVs encapsulating the sperm chromatin-added interphase egg extract, formed using the inverted emulsion method. The symbol τ denotes the duration of waiting time, and Δ denotes the volume of chloroform added to the lipid-dispersed oil. Magenta indicates lipid membrane (RhPE), and green indicates GFP dispersed in the egg extract. An inset shows a zoom-in of a typical GUV formed at τ = 0 min and Δ = 0%. Scale bar: 10 μm. (**B**) Number of GUVs plotted against τ (left) and Δ (right). (**C**) Proportion of GUVs with mean GFP intensity exceeding the computed threshold among the observed GUVs. (**D**) Diameter of all GUVs. (**E**) Number of GUVs with diameter larger than 5 μm. (**F**) Proportion of GUVs with diameter larger than 5 μm among the observed GUVs. Bars represent the mean (green) and Q1-Q3 quartiles (magenta). See "Materials and Methods" for the details on statistical analysis and Tables S1-12 for the results.

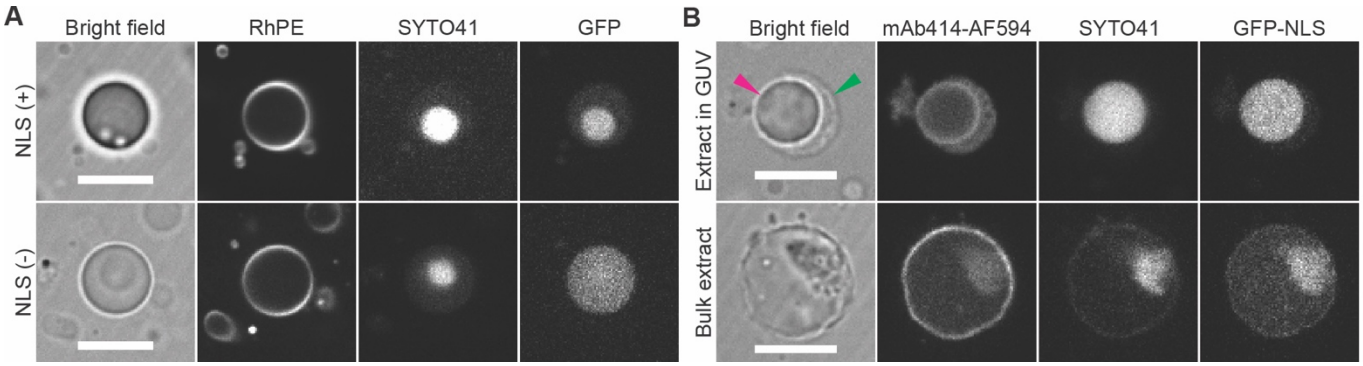

Fig. 3. Formation of nucleus-like structures in GUVs and immunostaining of nuclear pore complexes.

(**A**) GUVs after incubation for nuclear assembly reactions. RhPE: Lipid membrane, SYTO 41: nucleic acids (mainly DNA) stain. NLS(+): GFP with attached nuclear localization signals (NLS); NLS(-): GFP without NLS peptide. See Figs. S2-3 for additional examples. (**B**) A GUV containing a nucleus-like structure fixed with 2% glutaraldehyde and immunostained with mAb414-AF594 (top), and a nucleus formed under bulk condition, fixed and immunostained similarly (bottom). Arrowheads indicate GUV membrane (green) and nucleus-like structure (magenta). See Figs. S4-5 for additional examples. Scale bar: 10 μm.

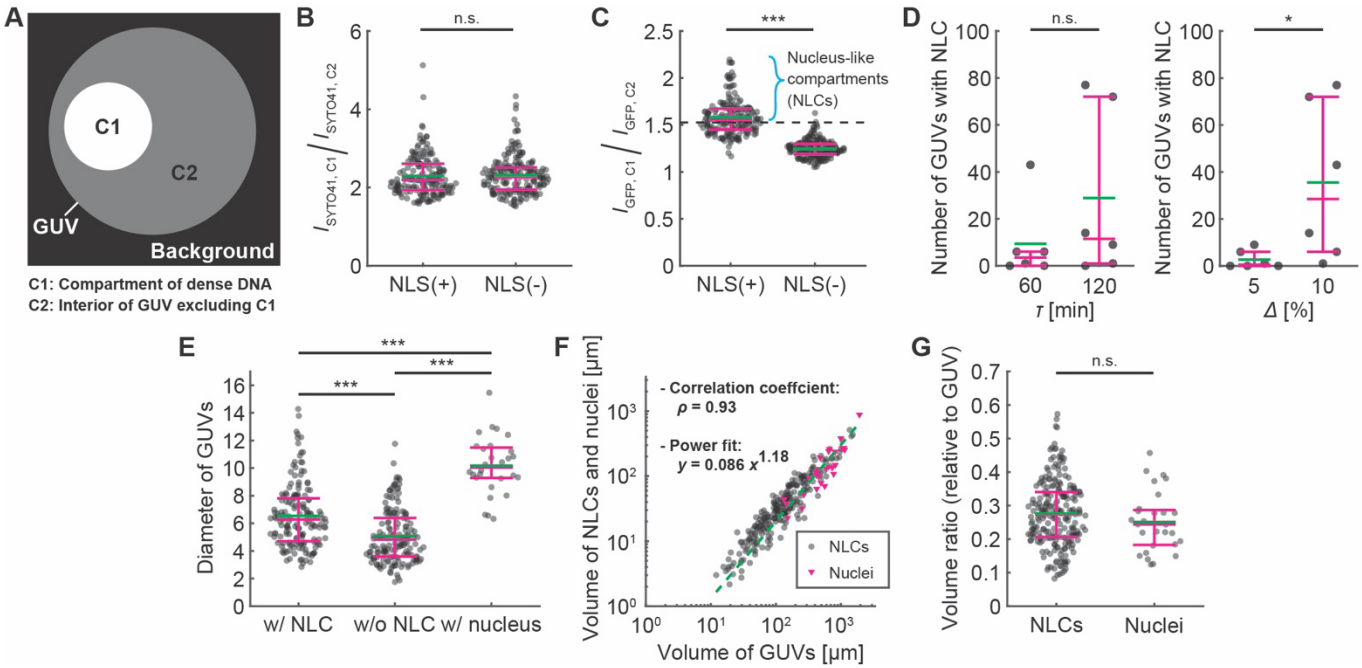

Fig. 4. Quantitative analysis of NLCs and nuclei formed in GUVs.
(**A**) Definition of internal compartments in a GUV. (**B**) Ratio of SYTO 41 intensity between C1 and C2 compartments in GUVs. $N = 182$ for NLS(+), $N = 193$ for NLS(-). (**C**) Ratio of GFP intensity between C1 and C2 compartments. The threshold of GFP-accumulation is mean + 3SD of NLS(-), indicated with a black dashed line (threshold value: 1.5). (**D**) Number of NLC-containing GUVs in the observed GUVs plotted against τ (left) and Δ (right). (**E**) Diameter of GUVs at τ = 120 min and Δ = 10%. GUVs containing an NLC are denoted as "w/ NLC", GUVs without NLC as "w/o NLC", and GUVs containing a nucleus as "w/ nucleus". N = 163 for w/ NLC and w/o NLC, N =28 for w/ nucleus. (**F**) Volumes of GUVs containing an NLC and that of NLCs are plotted with grey circles. Volumes of GUVs containing a nucleus are plotted in magenta triangles. The green dashed line is a result of power fit ($y = 0.086\,x^{1.18}$). $N = 229$ for NLCs, $N = 28$ for nuclei. (**G**) Ratio of the volume of NLCs and nuclei to the volume of the GUVs. In panels B-E and G, magenta bars indicate the Q1-Q3 quartiles, while a green bar indicates the mean. See "Materials and Methods" for the details on statistical analysis and Tables S13-20 for the results.

Supplementary Materials

Please see a separately submitted 'Supplementary Materials' for supplementary information: Supplementary Text, Figs. S1 to S12, Tables S1 to S23.